Deep Learning for landmarking on morphometry anatomical images

Le Van Linh[a,c,*], Beurton-Aimar Marie[a,1], Zemmari Akka[a], Parisey Nicolas[b,1]

[a]*University of Bordeaux, 351, cours de la Libration, 33405 Talence, France*
[b]*UMR 1349 IGEPP, BP 35327, 35653 Le Rheu, France*
[c]*Dalat University, Dalat, Lamdong, Vietnam*

Abstract

In recent years, deep learning, which has been introduced in the middle of the previous century for artificial intelligence, has risen strongly because of improvements in the computation. Deep learning has been applied to solve the problems in different domains such as computer vision, speech recognition, or languages translation. Among different type of deep learning architectures, convolutional neural networks have been most used in computer vision for image classification, object recognition, or key points detection and it has brought amazing achievements. In this work, we propose a convolutional neural network model to predict the key points (landmarks) on 2D anatomical biological images, specify beetle's images. Our proposed network is trained and evaluated on a dataset includes the images of collecting from 293 beetles. During the experiments, the network is tested in two ways: training from scratch and applying fine-tuning. The quality of predicted landmarks is evaluated by comparing with the manual landmarks which provided by the biologists. The obtained results are considered to be statistically good enough to replace the manual landmarks for the different morphometry analysis.

Keywords: Deep learning, CNN, fine-tuning, landmarks

---
[*]Corresponding author
  Email addresses: `van-linh.le@labri.fr` (Le Van Linh), `beurton@labri.fr`
(Beurton-Aimar Marie), `zemmari@labri.fr` (Zemmari Akka), `nicolas.parisey@inra.fr`
(Parisey Nicolas)
  [1]both authors contributed equally to this work.

1. Introduction

Deep learning is a part of machine learning. It allows the computational model composed of multiple layers to learn the representation of data. Each layer will extract the representation of input data which come from the previous layers, then it will compute a new presentation for the next layer. In a deep learning model, each layer may contain the different number of nodes, called *neurons* which have been inspired from the biological neural system. Actually, the computation at each layer is made by its neurons, and the operation at each neuron is also the same as a biological neural: the neuron receives different pieces of information and function properties to give the decision. Currently, deep learning has many kind of variant architectures such as Deep Neural Network (DNN), Convolutional Neural Network (CNN) or Recurrent Neural Network (RNN), which have been applied to different fields including computer vision, speech recognition, natural language processing, machine translation, ..., and each variant architecture has found success in a specific domain, i.e. DNN can be applied to solve the classification or data analysis, RNN give the best perform on language modeling, while CNN is widely applied in computer vision.

In the architectures of deep learning, CNN is a specific network for preprocessing data which have grid topology, i.e. time series (1-D) or images (2D). The name of the network is inspired by the convolution operation which is a kind of linear operation. Like the neural networks, a CNN consists of an input, an output layer, as well as one or multiple hidden layers. It has also the score function and the loss function at the end of the model. The computing of CNN affects on 3 dimensions of data: width, height, and depth. An input after being put on the network will be passed through a series of hidden layers before giving the outputs at the last layer. In a CNN, the hidden layers typically consist of convolutional layers, pooling layers, fully connected layer, ... From the first architecture [1] until now, many CNN architectures have been proposed and have succeeded in different tasks of computer vision such as image classification [1, 2, 3], object recognition [3, 4, 5].

In computer vision, key points detection is also an important field in image analysis. In this field, the algorithms try to find the key points (called interest points or landmarks) in the image. The landmarks are considered as the points in the image that are invariant when the image change i.e. rotate or translate. Depending the object, the number of landmarks may be different, as well as their position can be defined along the outline of the object or inside the object such as the landmarks on Drosophila wing [6] are stayed on the veins of the wings, but the landmarks on human ears [7] can be located on the ear edge or inside the Pimas of the ears. The detected key points are then used in different objectives of different domains, for example, they are used to recognize the seabed in geosciences; in computer vision, they are fundamental to detect the human face or human pose; in biology, the topography of the objects of an organism can be measured from the location of landmarks.

Early methods [8, 9, 6] mainly focused on the low level-vision of the image by applying the image processing techniques, and segmentation is most often the first and the most important step in the process. This task remains a bottleneck to compute the features of the complex image. Even if the interested object is easy to extract, the process may take a bit of time to extract the exciting features. The emergence of deep learning has seen success in other fields of computer vision and key points detection is also not an exception. It has been used to predict the fashion landmarks [10], human facial key points [11, 12], or ear landmarks [7].

In this work, we use deep learning, specific CNN, to predict the landmarks on biological anatomical images. The main idea consists of the designing and training a CNN on a dataset with manual landmarks. Like other CNNs, the features are extracted by using a group of different layer types (i.e. convolutional layer, pooling layer,. . .) followed by some fully connected layers to provide the prediction of the network. After designing, the proposed model will be trained on the dataset includes the images which are taken from 293 beetles. For each beetle, the biologists have taken images of five parts: *left and right mandibles, head, elytra, and pronotum* (Fig. 3). All the images are presented in the RGB

3

color model with two dimensions. Along with each image, a set of landmarks has been marked by experts which can be used as ground truth to evaluate the predicted landmarks. During the experiments, the proposed network has been trained on the dataset by applying two strategies. In the first strategy, the network is trained from scratch on each dataset; while in the second strategy, the training process has been modified to include a fine-tuning [13] stage. Besides, the value of Root Mean Square Error (RMSE) is used to compute the losses during two experiment processes.

The rest of this paper is organized as followed: Section 2 discusses the related works about determing the landmarks on 2D images. Then, a short overview about CNN and its components will be introduced in Section 3. Section 4 gives another approaches to augment the dataset. Section 5 shows the procedure of designing the network model. The first experiment of the network on each dataset is presented in Section 6. Section 7 presents a modification of training process and its experiment on datasets. Finally, the conclusion is given in Section 8.

2. Related works

In the middle of the previous century, deep learning [14] have been introduced as a method for artificial intelligence applications. However, several problems have appeared when taking into account it into real-world cases because of the limiting of memory or computing time. Nowadays, the improvement of computing capacities, both in memory size and in computing time with GPU programming, has opened a new perspective for deep learning. In recent years, deep learning architectures have achieved remarkable achievements in many tasks of different domains such as **computer vision** [1, 2, 3, 4, 5], **speech recognition** [15, 16], **language translation** [17, 18], **natural language processing** [14, 19, 20], ... In computer vision, deep learning, specifically with CNN, has been used to study the difficult tasks of image analysis such as image classification, or object detection. In the beginning, LeNet [1] has been

proposed and has been considered as the first architecture of CNN. LeCun et al. [1] have used LeNet in an application to classify the handwritten digits in cheques. LeNet has a standard of a CNN architecture which consists of convolutional layers, pooling layers, then followed by one or more fully connected layers. However, due to the lack of training data and computing power at that time, their network cannot perform the complex problems, i.e. large-scale image, or video classification. From that, many methods have been developed to response the encountered complexity in the training process of CNN. It must take into account AlexNet [2], which has significant improvement upon previous methods on image classification task. Basically, AlexNet [2] is similar to LeNet [1] but it has deeper structure and has been modified some parameters of layers such as using ReLU activation, adding Dropout layer to prevent the overfitting. AlexNet has famously won the ImageNet Challenge [2] in 2012. With the success of AlexNet, many models have been proposed to improve the performance of CNN, i.e. ZFNet [21], GoogLeNet [3], VGGNet [22], or ResNet [23]. From the comparison of architectures, easy to find that the networks are getting deeper by adding more layers and increasing the depth, e.g. ResNet, which won the champion of ILSVRC 2015, is deeper than AlexNet around 20 times. Clearly, the deeper models have provided better results but it also increases the complexity of the network, which makes the network be more difficult to optimize and easy to get overfitting.

With the success on classification and recognition tasks, CNNs have been applied for key points detection tasks and it has gained satisfactory results. Liu et al. [10] presented a method to predict the positions of functional key points on fashion items such as the corners of neckline, hemline and cuff. Yi Sun et al. [11] have proposed a CNN cascade to predict the facial points on the human face. The networks in their method have been separated into three levels of cascade to recognize the human face from the global to local view with the objective to increase the accuracy of predicted key points. In the same topic, Zhanpeng Zhang et al. [12] proposed a *Tasks-Constrained Deep Convolutional Network* to optimize facial landmarks detection. Along with detecting the facial landmarks,

5

their model has also detected a set of related tasks such as head pose estimation, gender classification, age estimation, or facial attribute inference. Shaoli Huang et al. [24] introduced a coarse-fine network, which composed of several coarse detector branches, to locate the keypoints and to estimate the human pose. Cintas et al. [7] introduced a network which enables to provide 45 landmarks on human ears. In the same context of key point detection, we develop a CNN to automate predicting some landmarks on beetle's anatomical.

3. Overview of Convolutional Neural Network

CNN is a feedforward network which takes the information following one direction from the inputs to the outputs. Currently, CNNs have many different variations, i.e. AlexNet [2], GoogLeNet [25], ResNet [23], but in general, it consists of convolutional and pooling layers which are stacked together to convolve and to down-sample the inputs. Then, they are followed by one or more fully connected layers to give the decision as the output of the network.

Fig. 1 shows an example of a CNN for classification problem. The network inputs directly an image to several stages of convolutional and pooling layers. Then, the representation is feed into three fully connected layers. A dropout layer is inserted after the second fully connected layer (it is repsented by some blue nodes). Finally, the last fully connected layer gives the category label for the input image. This architecture could be seen as the most popular one that we can find from the literature [1, 2]. However, several architectures have been proposed recurrently to improve the accuracy or to decrease the computation costs. In this section, we will mention to the most popular layers in a CNN: convolutional layers, pooling layers, and fully connected layers.

Convolutional (CONV) layers: use as a feature extractor by applying some learnable weights on the input images. The input image is convolved with the learnable weights in order to compute the new feature maps; then, the convolved results are sent through a nonlinear activation. In convolutional layer, the neurons are arranged into feature maps. All the neurons within a feature
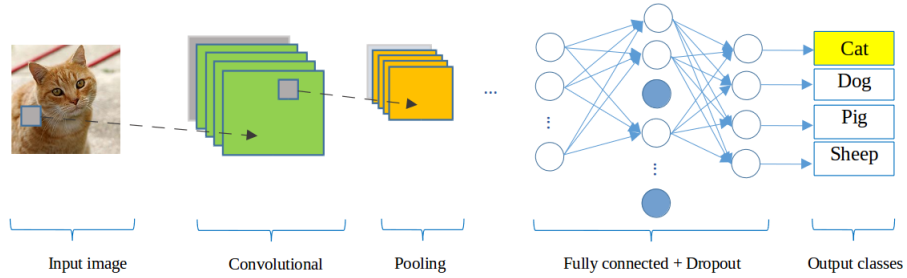
6

Figure 1: A CNN network for classification problem

map have constrained to be equal; however, different features maps within the same convolutional layer have different weights so that several features can be extracted at each location of an input image.

Pooling (POOL) layers : are mostly used to down-sampling the size of the input with the purpose to reduce the spatial resolution of the feature map to reduce the computation cost. Initially, it was common practice to use average pooling which propagates the average of all the input to the next layer. However, in more recent models [2, 26, 5], max pooling which propagates the maximum value (selecting the largest value) with a receptive field to the next layer. Fig. 2 illustrates the differences between max and average pooling. Give an input image of size 4×4, if applying a 2×2 filter and stride of two is applied, the output will be had the size of 2×2 for both cases. However, the value in each element of the output is different because the max pooling outputs the maximum values of the filter region, while average pooling outputs the average value of the same region.

Dropout (DROP) [27] is a specific layer, it is used to prevent the over-fit of a neural network. The term dropout mentions dropping the out units and their connections (incoming and outgoing)of a layer in the network. The units are dropped randomly with a probability p independent with other units. The idea of dropout is not limited to feed-forward neural nets. Applying dropout technique will make the network become a collection of thinned networks because a number of units are dropped randomly at each presentation of training phase.
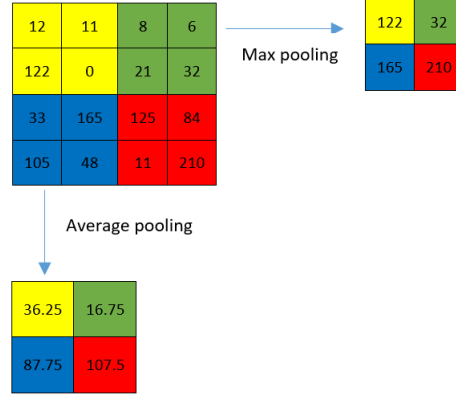
7

Figure 2: The results of different pooling

So, training a neural network with dropout looks like training a collection of the thinned networks. Normally, the dropouts layers are placed after the fully connected layers, but it is possible to use dropout after the pooling layers with creating some kind of images noise augmentation.

Fully connected (FC) layers: are usually followed the convolutional and pooling layers which used to extract the abstract feature representations. A CNN may have one or more fully connected layers. It interprets the feature representations and performs a function of high-level reasoning (i.e. giving classification score) by applying the activation functions. In practice, the last fully connected layer refers to the output of the network and choosing the activation function is depended on which kind of problem that network solve, i.e. we usually softmax activation function for a classification problem but it is not useful in a support vector machine.

To solve a problem by using deep learning, besides designing the network architecture then training dataset is also a very important thing. The success stories [2, 23] have proved that CNN models work better with a large dataset. However, data in practice has usually not enough and we need to augment the data by applying some generation techniques (i.e. rotate, translate, flip the images). In the next section, we describe the procedure to augment our dataset,

which has been considered as a small one.

4. Data augmentation

The nature of deep learning algorithm is training the model on dataset re-
peatedly to reach the best accuracy. So, providing a large dataset will provide
more learning cases for the model and it will clearly improve the learnable of
the network. Unfortunately, we do not always have enough data for training in
practice. One way to solve this problem is to create fake data from real data
and to add it to the training set. Dataset augmentation has been a particularly
effective technique for a specific problem. For example, the operations like trans-
lating, rotating or scaling the images have also effective in image classification
problem. The fake images may be generated by translating (rotating or scaling)
in each direction. Besides, injecting noise in the input can also see as a form
of data augmentation. Our case is also not an exception, we work on a small
dataset of beetles with 293 images of beetles (for each anatomical part). This
number is really modest to apply deep learning. So, an augmentation method
has been described in this section to enlarge our dataset.

In our dataset, all the images are taken with the same camera in the same
condition with a resolution of (3264×2448). Each image has a set of manual
landmarks provided by biologists, i.e, each pronotum has 8 landmarks, each
head has 10 landmarks (Fig. 3). Applying CNNs to train each part with a
small number of images to reach good results is impossible. So, we need to
augment the dataset before training the networks. Firstly, we have found that
the original solution of the images (3264×2448) are heavy for the neural network.
For performance considerations, in most of CNNs [7, 28, 11], the size of the input
is limited to (256×256) pixels, so we have decided to down-sampling the images
to a new resolution (256×192) (to respect the ratio between x and y). Of course,
the coordinates of manual landmarks have been also scaled to fit with the new
resolution of the images. In the usual way, the transformations have been used
to augment the dataset (i.e rotation, translation,. . .) but the analysis of image

9

by CNN is most often translation and rotation invariant. Therefore, two other procedures have been imaged to increase the number of images in the dataset (256×192).
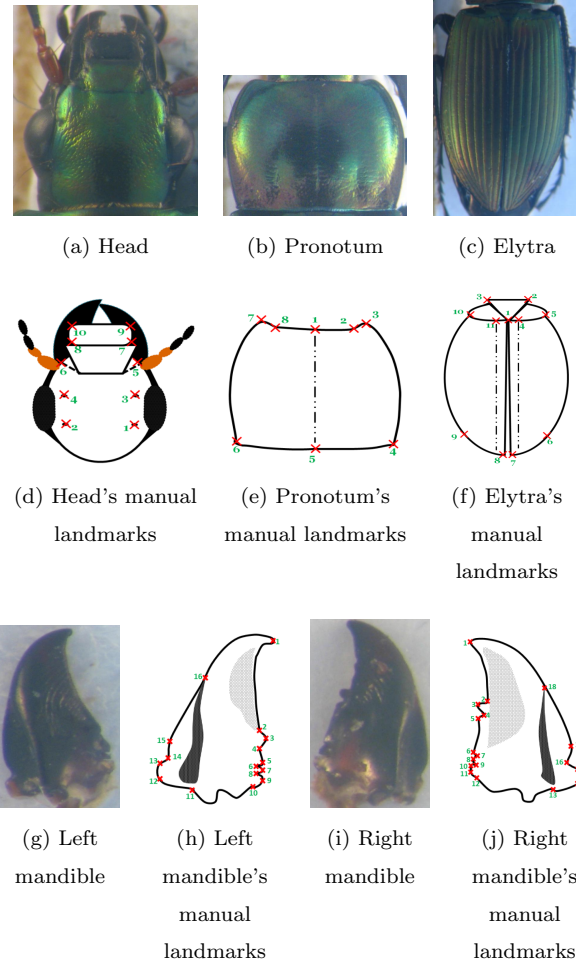

(a) Head   (b) Pronotum   (c) Elytra

(d) Head's manual landmarks   (e) Pronotum's manual landmarks   (f) Elytra's manual landmarks

(g) Left mandible   (h) Left mandible's manual landmarks   (i) Right mandible   (j) Right mandible's manual landmarks

Figure 3: The anatomicals of beetle and their manual landmarks

The first procedure is to change the value of a color channel in the original image to generate a new image. According to that, a constant is added to one of the RGB channels each time it is used for training. Each constant is sampled in a uniform distribution $\in [1, N]$ to obtain a new value caped at 255. For

10

example, Fig. 4 shows an example when we added a constant $c = 10$ to each channel of an original image. Following this way, we can generate three version from an image.
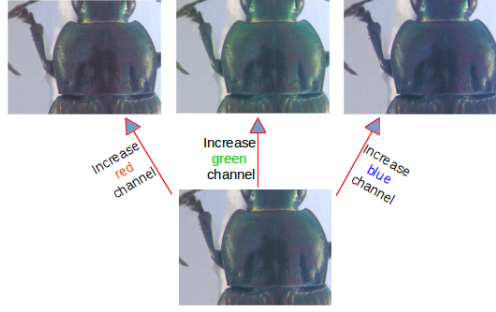

Figure 4: A constant $c = 10$ has been added to each channel of an original image

In the second procedure, we have applied the opposite procedure to the first one. Instead of adding the value, we separate the channels of RGN into three gray-scale images as the network works on single channel images (Fig. 5). At the end of the processes, we are able generate six versions from an original image. In total, we have $293 \times 7 = 2051$ images for each anatomical part of beetle (an original image and six generated images). However, we have not used all images for training and validation. So, we have chosen 260 original images and their generations (1820 images) of each dataset for training and validation processes, the remaining images (33 original images) are used for test process.
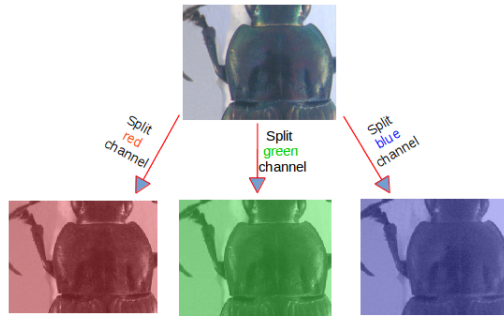

Figure 5: Three channels (red, green, blue) are separated from original image

In practical, to obtain a fast convergence during the computing, it is useful to normalize the brightness of the images to $[0, 1]$ instead of $[0, 255]$ and the coordinates of the landmarks have been also normalized [29].

5. Network architectures designing

From the beginning of CNN, LeNet [1] can be considered as the first one, which has used to classify digits on hand-written numbers on cheques. The network is very simple by stack together the convolutional layers and max-pooling layers followed by full connected layers. Because of the limit of the resources at that time, this model is also constrained by the availability of computing. Until 2012, when computing resources are improved, AlexNet [2] was born and it has won the challenge by reducing the top-5 error in ImageNet challenge. AlexNet had a similar architecture as LeNet but it was deeper, bigger. Besides, the activation functions have been changed from Sigmoid [30] to ReLU [31] which have been proved more improvement in computing time. Additional, it had supplement the dropout layers to control overfitting. Based on the idea of the improvement, we have tried to design an architecture for landmarking on beetle images. This work is beginning with trying three network models before deciding the final architecture. Like other CNN models, we have employed the classical layers to construct the models, i.e., convolutional layers, maximum pooling layers, dropout layers and full-connected layers.

The first architecture is very classical one, it receives an image with the size of $(1 \times 192 \times 256)$ as the input. Then, the network consists of three repeated structures of a convolutional layer followed by a maximum pooling layer. Most of CNNs, the hyperparameters of convolutional layers have been set to increase the depth of the images from the first layer to the last layer. That is reflected in the setting of the number of filters at each convolutional layer. So, the depths of convolutional layers increase from $32, 64$, and 128 with different size of the kernels: (3×3), (2×2) and (2×2), respectively. Inserting pooling layers after a convolutional layers is a common periodcally. The pooling layer effects to

progressively reduce the spatial size of the representation to reduce the number
of parameters, computation in the network, and it also controls over-fitting.
The operation of pooling layers is independent on every depth slice of the input.
The most common form is a pooling layer with filters of size (2×2) and a stride
of 2. It downsamples every depth by 2 along width and height of the input.
Thefore, all the kernels of maximum pooling layers have the same size of (2×2)
with a stride of 2 as usual. At the end of the model, three full-connected layers
have been added to extract the global relationship between the features and
to procedure the outputs. The first of two full-connected layers are set to non-
linearity to make sure these nodes interact well and take into account all possible
dependencies at the feature level. The outputs of the full-connected layers
are $500, 500$ and 16. The output of the last full-connected layer corresponds
to the coordinates (x and y) of 8 landmarks which we would like to predict.
Fig. 6 shows details of the first model: The orange rectangles represent for
convolutional layers while the yellow rectangles represent for maximum pooling
layers and three full-connected layers with their parameters are presented at the
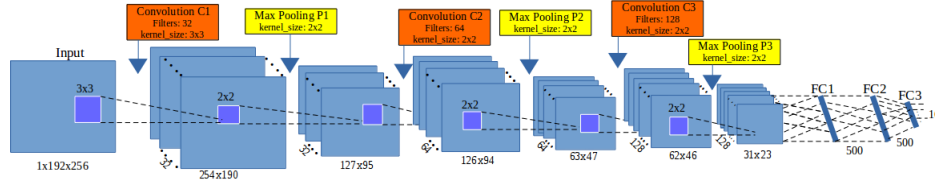end of the model.

Figure 6: The architecture of the first model

The second architecture is modified from the first model. The layers are kept
the same as the first one but the outputs of the first of two full-connected layers
are changed from 500 (in the first model) to 1000 (Fig. 7). Increasing the value
at full-connected layers is hoping to obtain more features from convolutional
layer and to prevent the over-fitting.

To build the third architecture, we have used the definition of *elementary
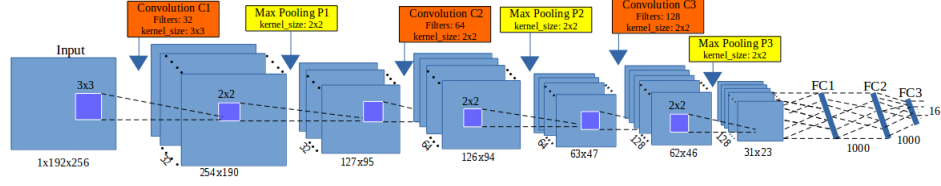block*. An elementary block is defined as a sequence of convolution (C_i), maxi-

Figure 7: The architecture of the second model

mum pooling (P_i) and dropout (D_i) layers (Fig. 8). This significantly reduces overfitting and gives major improvements over other regularization methods [27]. The idea of dropout is to include some variations between different runs. During training phase, dropout samples are done from an exponential number of different "thinned" network. At test phase, it is easy to approximate the effect of averaging the prediction of all thinned networks by simply using a single unthinned network with smaller weights. So, we have modified the architecture by combining some *elementary blocks*.
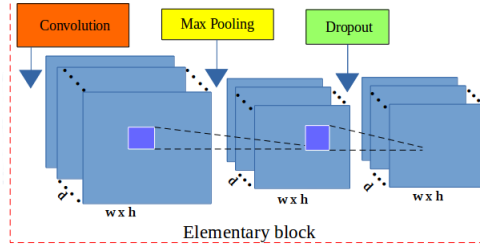

Figure 8: The layers in an elementary block

Fig. 9 illustrates the layers in the third architecture. For our purpose, we have assembled **3 elementary blocks**. The parameters for each layer in each elementary block are as below, the list of values follows the order of elementary blocks ($i = [1..3]$):

- CONV layers:

    - Number of filters: $32, 64$, and 128

    - Kernel filter sizes: $(3 \times 3), (2 \times 2)$, and (2×2)

14

– Stride values: $1, 1,$ and 1

– No padding is used for CONV layers

- POOL layers:

    – Kernel filter sizes: $(2 \times 2), (2 \times 2),$ and (2×2)

    – Stride values: $2, 2,$ and 2

    – No padding is used for POOL layers

- DROP layers:

    – Probabilites: $0.1, 0.2,$ and 0.3

Three full-connected layers (FC) are kept the same as the second architecture: FC1 and FC2 have 1000 outputs, the last full-connected layer (FC3) has 16 outputs. As usual, a dropout layer is inserted between FC1 and FC2 with a probability equal to 0.5.
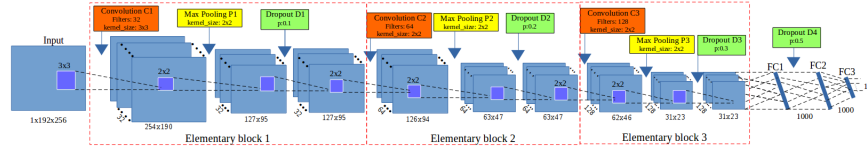

Figure 9: The architecture of the third model

The core of CNN is training over iteration. There are many ways to optimize the learning algorithm, but gradient descent [29] is currently a good choice to establish the way of optimizing the loss in neural network. The core idea is following the gradient until we statify with the results will remain the same. So, we have chosen gradient descent in the backward phase to update the values of learnable parameters and to increase the accuracy of the network. The networks are designed with a small sharing learning rate and a momentum. The learning rate is initialized at 0.03 and stopped at 0.00001, while the momentum is updated from 0.9 to 0.9999. Their values are updated

15

over training time to fit with the number of epochs [2]. The implementation of the architectures have been done on Lasagne framework [32] by Python. For more information about the model, you can see at our repository on GitHub: `https://github.com/linhlevandlu/CNN_Beetles_Landmarks`

6. Experiments and results

Before widely applying to all anatomical parts, we have firstly tried with pronotum part to evaluate the performance. The networks have been trained in $5,000$ epochs on Ubuntu machine by using NVIDIA TITAN X cards. The set of images that used for training and validation are merged together. During the training, the images are chosen randomly from the dataset with a ratio of 60% for training and 40% for validation. The training step takes into account a pair of information (*images, manual landmarks coordinates*) as training data. In the context of deep learning, landmark prediction can be seen as a regression problem. So, we have used Root Mean Square Error (RMSE) to compute the loss of implemented architectures. At the test phase, images without landmarks are given to the trained network to produce output coordinates of the predicted landmarks. The results then evaluated by comparing with the manual landmarks coordinates provided by biologists which have been seen as ground truth.

Fig. 10 shows the training errors and the validation errors during traning phase of the first architecture. The blue curve presents the RMSE errors of training process while green curve is the validation errors. Clearly, over-fitting has appeared in the first model. The training losses are able to decrease but the validation losses are stable. In the second model (Section 5), we have modified the parameters of full-connected layers to prevent the over-fitting but it seems that this solution is still not suitable and the results are also the same with the first architecture.

---

[2]An epoch is a single pass through the full training set
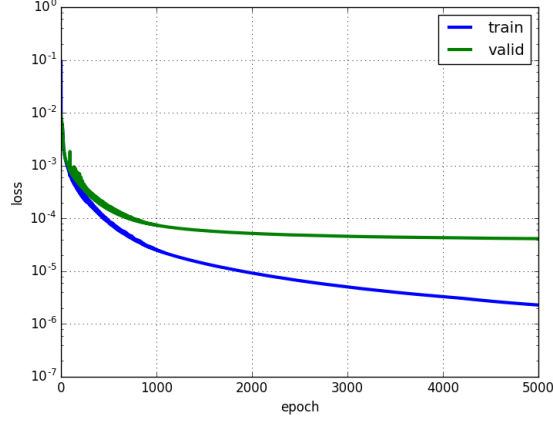
16

Figure 10: The training and validation losses of the first model

Then, we have continued to train the third model on the same dataset of pronotum images. Fig. 11 illustrates the losses during the training of the third model. As the same meaning in Fig. 10, the blue line is training loss, the green line is validation loss. In the opposite with two previous models, the losses are different (far) from the beginning but after several epochs, the loss values become more proximate and the over-fitting problem has been solved. This proves that adding dropout layers to build the elementary blocks have been effects to prevent over-fitting and contributory improve the accuracy of the model. *So, we have decided to keep the architecture of the third model for our landmarking problem.*

In order to have the predicted landmarks for all pronotum images (instead of only 33 images), we have applied *cross-validation* to choose the test images, called *round*. For each time, we have chosen a different fold of 33 images as testing images, the remaining images are used as training and validation images $(293/33 \approx 9$ rounds). Following that, the network will be trained with different datasets, then the trained model will be used to predicted the lanmarks on the images in the corresponding test set. Table. 1 resumes the losses of 9 rounds when we trained the third model on pronotum images. Clearly, the training
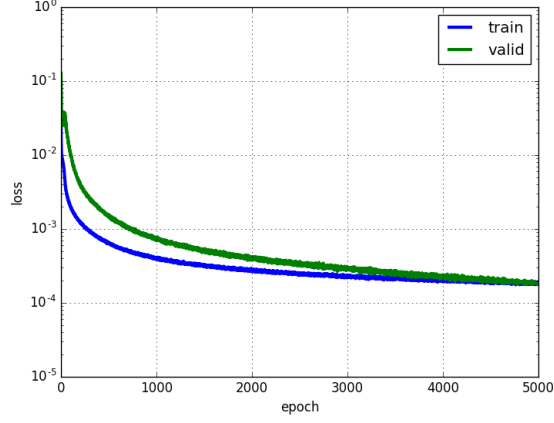
Figure 11: The training and validation losses of the third model

loss/validation loss among rounds are not so large and the RMSE values are
looking pretty good ($\approx 1.7 - 2.1$ pixels).

Round	Training loss	Validation loss
1	0.00018	0.00019
2	0.00019	0.00021
3	0.00019	0.00026
4	0.00021	0.00029
5	0.00021	0.00029
6	0.00019	0.00018
7	0.00018	0.00018
8	0.00018	0.00021
9	0.00020	0.00027

Table 1: The losses during training the third model on pronotum images

To evaluate the coordinates of predicted landmarks, the correlation metrics
have been computed the correlation between the manual landmarks and their
corresponding predicted one. Table. 2 shows the correlation scores of 3 metrics
(using *scikit-learn* [33]), i.e, coefficient of determination (r^2), explained variance

18

(EV), and Pearson correlation. All of three metrics have the same possibility. The best score is 1.0 if the correlation data is good, lower values are worse. It means that our predicted coordinates are very close with the ground truth. However, the measure is not enough good to provide a useful result to biologists. Moreover standing on the side of image processing, we are looking forward to seeing the predicted coordinates than the statistical results.

Metric	r^2	EV	Pearson
Score	0.9952	0.9951	0.9974

Table 2: Correlation scores between manual landmarks and predicted landmarks

The main goal of computing is to predict the coordinates of landmarks, so the distances (in pixels) between the coordinates of manual landmarks and corresponding predicted landmarks have been taken into account on all images. Then, the average of distances are computed by landmarks. Table. 3 shows the average distances by landmarks on all images of pronotum dataset. With images of resolution 256×192, we can consider that an error of 1% corresponds to 2 pixels that could be an acceptable error. Unhappily, our results exhibit average distance of 4 pixels in the best case, landmark 1 and more than 5 pixels, landmark 6. Other error distances are more than 2% pixels.

Fig. 12 shows the distribution of the distances on the first landmark of all images. The accuracy based on the distance in each image can be separated into three spaces: the images have the distance less than average value (4 pixels): 56.66%; the images have the distance from average value to 10 pixels (5% acceptable errors): 40.27%; and the images have the distance greater than 10 pixels: 3.07%.

To illustrate this purpose, Fig. 13 shows the predicted landmarks on two test images. One can note that even some predicted landmarks (Fig. 13a) are closed to the manual ones, in some case (Fig. 13b) the predicted ones are far from the expect results. This result explains why the average distance by landmarks are enough good while some predicted landmarks are so far from the manual one.

19

Landmark	Distance (in pixels)
1	4.002
2	4.4831
3	4.2959
4	4.3865
5	4.2925
6	5.3631
7	4.636
8	4.9363

Table 3: The average distances on all images per landmark on pronotum images.
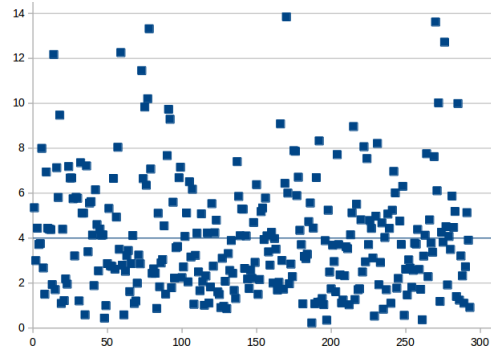

Figure 12: The distribution of the distances on the first landmark. The blue line is the average value of all distances.

So, the next step has been dedicated to the improvement of these results.

(a) Image with well-predicted
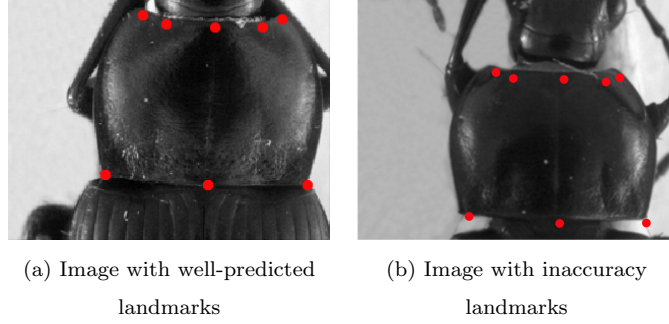landmarks

(b) Image with inaccuracy
landmarks

Figure 13: The predicted landmarks, in red, on the images in test set.

From the success of the third architecture on pronotum dataset, we apply the same procedures (data augmentation, training,...) on other parts of beetle: *left mandible, right mandible, elytra, and head*. However, we have modified the number of output of the last full-connected layer to adapt with each dataset before training. According, the values at the last full-connected layer are set to 32, 36, 22 and 20 outputs corresponds to 16, 18, 11 and 10 landmarks on left mandible, right mandible, elytra and head, respectively. Of course, we have also applied cross-validation to select testing data to get all predicted landmarks for all images in each dataset. Then, the quality of predicted landmarks are evaluated by comparing with the corresponding manual landmarks (distance computation). Table. 4 shows the average distances on each landmark of elytra, head, left and right mandibles anatomical, respectively. Comparing with the average distances on the pronotum part, the average distances on elytra and head parts are very close, but a little bit far on the mandible parts.

7. Resulting improvement by fine-tuning

The proposed network (third architecture) presented in Section 5 have been trained from scratch on five datasets of beetles (left mandible, right mandible, pronotum, elytra, and head). At the first step, the network was able to predict

21

Landmark	Distance (in pixels)			
	Right mandible	Left mandible	Elytra	Head
1	9.4981	9.1267	3.8669	5.528
2	7.1657	6.7198	3.973	5.1609
3	7.242	6.8704	3.9166	5.3827
4	7.0436	6.7719	3.8673	5.0345
5	7.1599	7.125	4.0151	4.8393
6	7.5699	6.9441	4.8426	4.4516
7	7.4251	7.3158	5.2125	4.7937
8	7.6636	7.4142	5.4685	4.5322
9	7.7906	7.5846	5.2692	5.1412
10	8.0197	7.6349	4.0709	5.0564
11	8.314	7.6873	3.9896	-
12	8.1564	8.4248	-	-
13	8.8879	7.9983	-	-
14	9.1842	7.4919	-	-
15	8.7875	7.7903	-	-
16	8.3141	8.5198	-	-
17	8.2866	-	-	-
18	8.8928	-	-	-

Table 4: The average distances on all images per landmark on left mandible, right mandible, elytra and head images.

the landmarks on the images. But as we have discussed, even if the strength of the correlation seems to validate the results, when we display the predicted landmarks on the images, the quality of the predicted coordinates are also not enough precise, and the average error are also still high (of course, we have the distances are higher than the average distances).

In order to reach more acceptable results for biologists, we have broadened model with another step of deep learning: **transfer learning**. That is a method enables to re-uses the model developed for a specific task/dataset to lead another task (called *target task*) with another dataset. This process allows rapid process and improves the performance of the model on the target task [34]. The most popular example has been given with the project ImageNet of Google [35] which has labeled several millions of images. The obtained parameter values which can be used in another context to classify another dataset, eventually very different dataset [36]. The name of this procedure to re-use parameters to pretrain a model is currently called **fine-tuning**.

Fine-tuning does not only replace and retrain the model on the new dataset but also fine-tunes the weights of a trained model by continuing the backpropagation. Unfortunately, some rapid tests have shown that re-using ImageNet features has not been relevant for our application. We have designed a way to reproduce the method with our own data. It is worth noting that of course the size of data to pre-train has drastically decreased. For our pre-training step, the network has been trained on the whole dataset including the images of three parts of beetle *i.e pronotum, elytra and head*. Then, the trained model has been used to fine-tune and test on each dataset.

7.1. Data preparation and training

The images training dataset is combined from the images of three sets: *pronotum, elytra, and head* (after augmentation). When applying the training from the scratch, we have used cross-validation to select the data (9 folds). It means that for each dataset, we have some different training data and corresponding testing data. So, the images that use to train the model are just select

23

from one of the folds in each dataset. Specifically, we have taken $1,820$ images of each part. In total, it includes $5,460$ images ($260 \times 7 \times 3$).
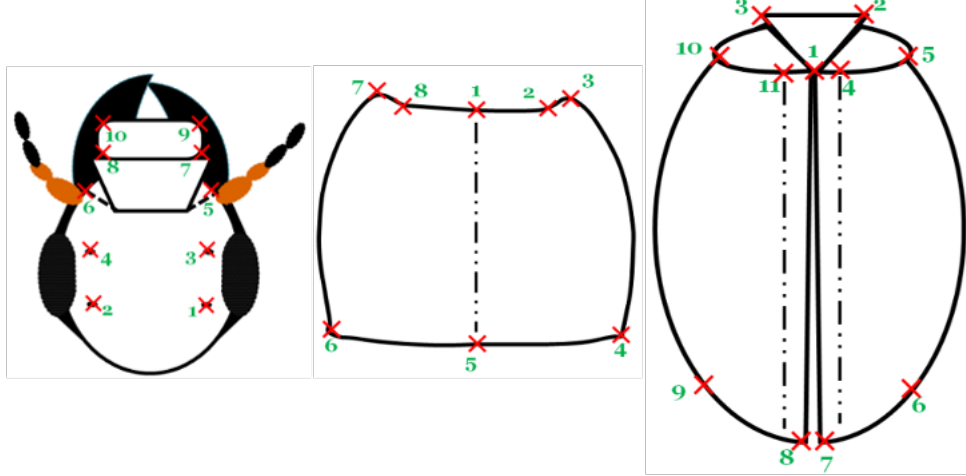

Figure 14: A presentation of head, pronotum and elytra part with corresponding manual landmarks

However, another problem has been appeared when we combined the images from different dataset. That is the different number of landmarks on each part: 8 *landmarks on pronotum part,* 10 *landmarks on head part, and* 11 *landmarks on elytra part.* Fig. 14 shows the possition of the landmarks on each part. Because of the meaning of landmarks on each anatomical part for biologists, we cannot insert the landmarks arbitrary. So, we have decided to keep the landmarks on pronotum as reference and to remove the landmarks on elytra and head parts instead of adding. We kept 8 (landmarks) as a reference number, then we have removed the supernumerary when it is unnecessary. Specifically, we have removed three landmarks on the elytra part ($1^{st}, 6^{th}, 9^{th}$), and two landmarks on the head part ($5^{th}, 6^{th}$).

During training the proposed architecture on the combined dataset, the parameters of the network (learning rate, momentum, . . .) are kept the same as training from scratch but the number of epochs are increased to $10,000$ instead of $5,000$ to achieve better learning on the parameters (weights). Additional,

24

we have shuffled the training data because the neural network learns the faster from the most unexpected sample. It is advisable to choose a sample at each iteration that is the most unfamiliar to the system. Shuffling the examples will be helped the model works with different anatomical parts rather than the same anatomical samples in each training time.

7.2. Fine-tuning on each dataset

The combined dataset then used to train the third architecture with 16 outputs (8 landmarks). Then, the trained model is used to fine-tuning on each dataset. To compare the result with the previous one, we have also fine-tuned the trained model with different dataset by applying cross-validation. Firstly, we consider on the losses during fine-tuning. *For example*, Table. 5, 7, 9 show the losses during fine-tuning on pronotum, elytra, and head dataset, respectively. Comparing with the losses when we trained the model from scratch, *i.e.* on pronotum, the validation losses of all round in this scenario have been significantly decreased (around 40%).

On each part, the landmarks are predicted on the test images. Then, the average error based on the distances between predicted and corresponding manual landmarks have been also computed. Tables. 6, 8, 10, 11, and 12 show the average distances per landmark on pronotum, elytra, head, left and right mandibles dataset, respectively. **From scratch** columns remind the previously average distances. **Fine-tune** columns present the new average distances after applying fine-tuning on each part. It is clearly shown that the result of predicted landmarks with the help of fine-tuning is more precise than training from scratch. For example, the average distance at each landmark has decreased. Additional, when comparing the average distances between two processes, the worse case of fine-tuning process is still better than the best case of training from scratch.

In another view, Fig. 15 shows the comparison of the average distance distributions on each dataset in two procedures (from scratch and fine-tuning). In which:

Round	Training loss	Validation loss
1	0.00019	0.00009
2	0.00018	0.00010
3	0.00018	0.00010
4	0.00019	0.00008
5	0.00019	0.00009
6	0.00018	0.00008
7	0.00019	0.00008
8	0.00018	0.00006
9	0.00018	0.00009

Table 5: The losses during fine-tuning model on pronotum dataset

#LM	From scratch	Fine-tune
1	**4.00**	**2.49**
2	4.48	2.72
3	4.30	2.65
4	4.39	2.77
5	4.29	2.49
6	**5.36**	**3.05**
7	4.64	2.68
8	4.94	2.87

Table 6: The average error distance per landmark of two processes on pronotum images

Round	Training loss	Validation loss
1	0.00020	0.00006
2	0.00020	0.00006
3	0.00021	0.00006
4	0.00021	0.00006
5	0.00019	0.00006
6	0.00019	0.00006
7	0.00018	0.00005
8	0.00020	0.00006
9	0.00019	0.00006

Table 7: The losses during fine-tuning model on elytra dataset

#LM	From scratch	Fine-tune
1	**3.87**	2.34
2	3.97	2.27
3	3.92	2.27
4	**3.87**	**2.25**
5	4.02	2.27
6	4.84	3.14
7	5.21	3.14
8	**5.47**	3.29
9	5.27	**3.42**
10	4.07	2.49
11	3.99	2.30

Table 8: The average error distance per landmark of two processes on elytra images

Round	Training loss	Validation loss
1	0.00022	0.00007
2	0.00022	0.00007
3	0.00023	0.00008
4	0.00023	0.00008
5	0.00022	0.00008
6	0.00023	0.00007
7	0.00022	0.00008
8	0.00023	0.00007
9	0.00024	0.00008

Table 9: The losses during fine-tuning model on head dataset

#LM	From scratch	Fine-tune
1	5.53	**3.03**
2	5.16	2.94
3	**5.38**	2.96
4	5.03	2.88
5	4.84	2.76
6	**4.45**	2.67
7	4.79	2.29
8	4.53	**2.20**
9	5.14	2.57
10	5.06	2.44

Table 10: The average error distance per landmark of two processes on head images

- **Blue** curves: present for the average distances on each landmarks when we train the model from scratch.

- **Orange** curves: describe for the average distance on each landmark when we fine-tune the trained model.

- **Black** curves (in the case of left and right mandibles): illuslate for the average distances when we applied the image processing procedures to predict the landmarks on segmentable images.

The fine-tuning process has improved the results of the proposed architecture on both 5 datasets: left, right mandible, pronotum, elytra and head. All the average distances are significantly decreased. Specially, the results have been improved $\approx 26.9\%$ on left mandible, $\approx 22.8\%$ on right mandible, $\approx 40.3\%$ on pronotum, $\approx 39.8\%$ on elytra, and $\approx 46.4\%$ on head part based on considering the average distances per landmark. Addition, in the cases of pronotum and head part, even if we plus the average distance and its standard deviation, the

| #LM	From scratch	Fine-tune
1	9.1267	6.7655
2	6.7198	5.2952
3	6.8704	5.3468
4	6.7719	5.332
5	7.125	5.4391
6	6.9441	5.3004
7	7.3158	5.5314
8	7.4142	5.6486
9	7.5846	5.8864
10	7.6349	5.9245
11	7.6873	5.972
12	8.4248	6.5755
13	7.9983	6.1067
14	7.4919	5.6307
15	7.7903	5.8522
16	8.5198	7.174

Table 11: The average error distance per landmark of two processes on left mandible images

| #LM	From scratch	Fine-tune
1	9.4981	6.3236
2	7.1657	5.1347
3	7.242	5.1613
4	7.0436	5.0537
5	7.1599	5.1372
6	7.5699	5.301
7	7.4251	5.2064
8	7.6636	5.5168
9	7.7906	5.6858
10	8.0197	5.7495
11	8.314	6.1975
12	8.1564	6.1898
13	8.8879	6.7612
14	9.1842	7.0694
15	8.7875	6.5293
16	8.3141	6.1147
17	8.2866	6.2881
18	8.8928	6.8367

Table 12: The average error distance per landmark of two processes on head images
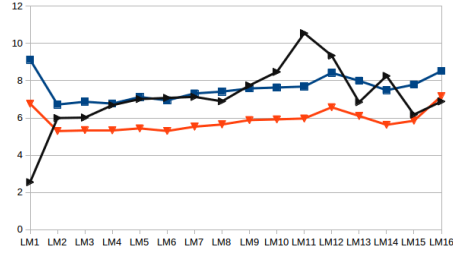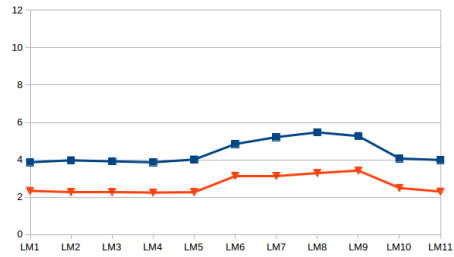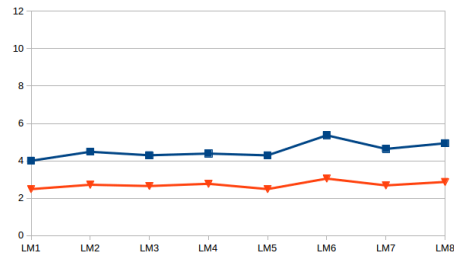
(a) Left mandible
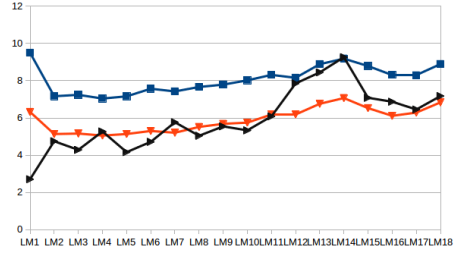
(b) Right mandible
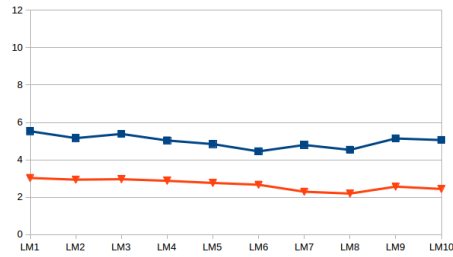
(c) Head

(d) Elytra

(e) pronotum

Figure 15: The distribution of average distances on each landmark of each beetle's anatomical

results are also less than the result when we trained the model from scratch. For segmentable images, we have a comparison between the results of deep learning and early method where we have applied image processing techniques to predict the landmarks [37]. Clearly, the result with fine-tuning has improved the location of estimated landmarks. Even the average distances which obtained from scratch training are still high but they are more stable than the results from the early method: most of the average distance(or landmarks) of left mandibles are less than the results of the early method, while the average distances are very closed in the case of right mandibles.

To compare the results between image processing procedures and deep learning, we have run the test on an image of all parts in both methods. Then, we have calculated the distances between manual and predicted landmarks (in both cases). Fig. 16 shows the locations of manual and predicted landmarks on each beetle's part from both two methods. In these images, the **red points** present the manual landmarks, the **yellow points** are estimated landmarks from image processing procedures and the **green points** are predicted landmarks which provided by deep learning.

Fig. 17 shows the distances of each part that we have obtained. In these charts, the **blue lines** present the distances when we apply the calculation on image processing procedures; the **orange and yellow lines** show the distances with deep learning: training from scratch and fine tuning, respectively. As described in [37], we have combined some image processing procedures to output the predicted landmarks and this has become also a disadvantage of this method. If one procedure of them provides a bad result, it will affect the final result, i.e. if the result of segmentation step is bad, it seems that can not provide the output. In all beetle's anatomical, the mandibles are considered as the easy case to segment because the images are clear (they just contains the mandibles); while other parts are much noise, besides the main objects they have also the subcomponents of beetle, i.e. leg, antennae, ... That explains why we have obtained good results on mandibles but bad results on head, elytra, and pronotum part when applying the image processing procedures. In the opposite side,

30

(a) Left mandible

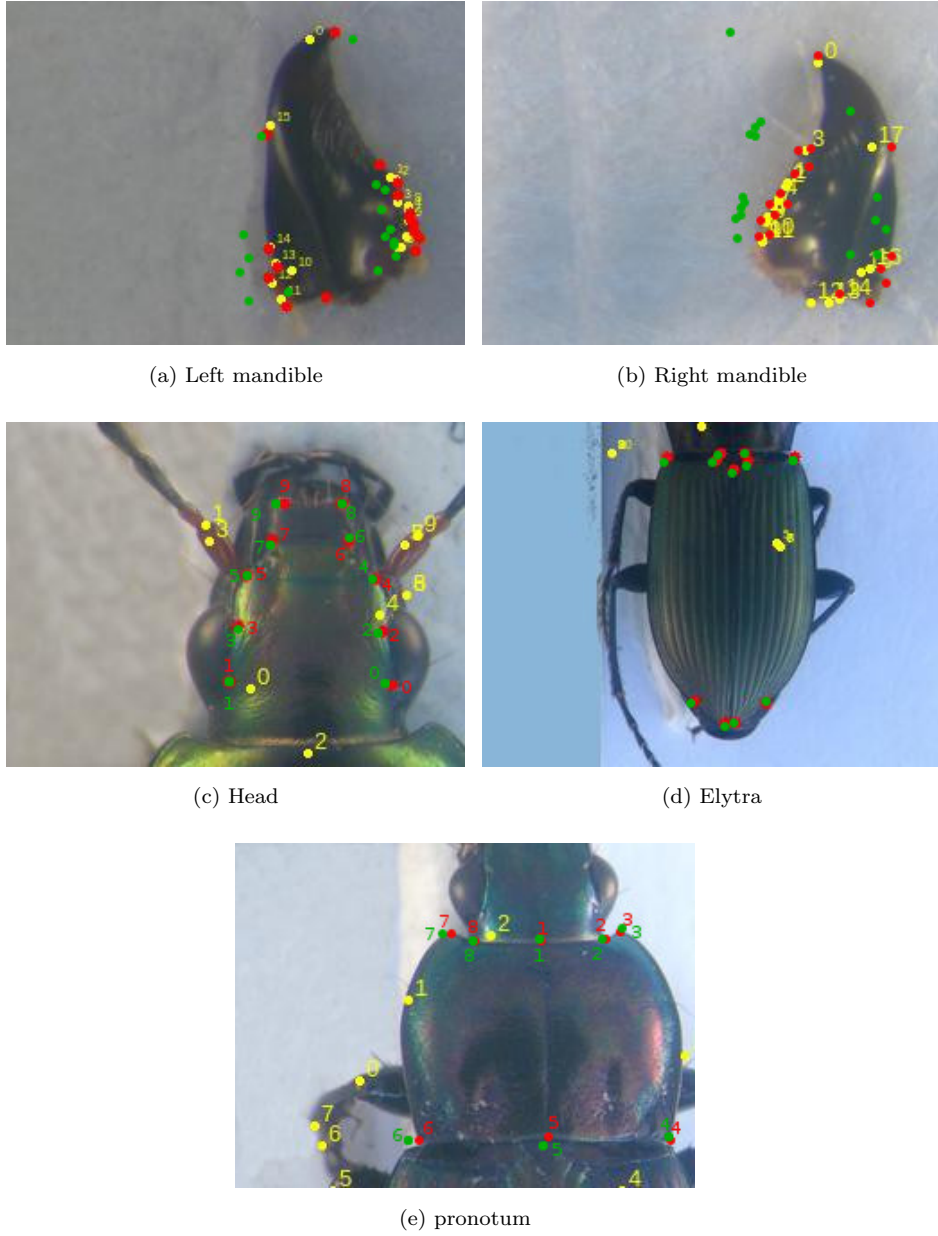(b) Right mandible

(c) Head

(d) Elytra

(e) pronotum

Figure 16: The presentation of manual and predicted landmarks on each beetle's part by applying two methods: image processing procedures and deep learning

the results with deep learning, either training from scratch or fine-tuning, are very stable (Fig. 17). In the case of mandibles, which have good results from image processing techniques, then the results from deep learning are not much difference.
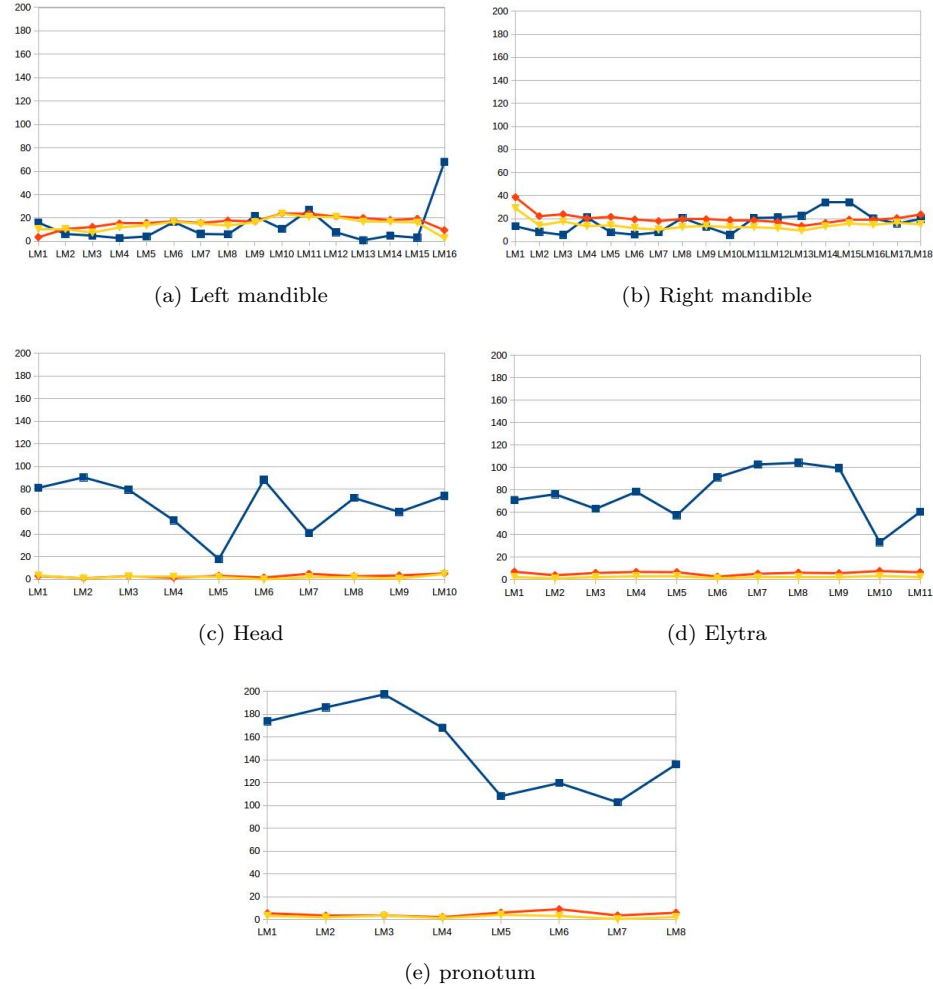

(a) Left mandible

(b) Right mandible

(c) Head

(d) Elytra

(e) pronotum

Figure 17: The distances between manual and predicted landmarks of a test image when applying different techniques of each beetle's anatomical

8. Conclusion

In this work, we have presented how to apply convolutional neural network to predict the landmark on 2D anatomical images of beetles. After going through many trial models, we have presented a convolutional neural network for automatic detection landmarks on anatomical images of beetles which includes the repeated of some elementary blocks (an elementary block consists of a convolutional layer, a max pooling layer, and a dropout layer) followed by fully connected layers. Then, the proposed model have been trained and tested by using two strategies: *train from scratch* and *fine-tuning*.

In our case, the size of dataset is limited. Therefore, we have applied the image processing techniques to augment dataset. The predicted landmarks have been evaluated by calculating the distance between manual landmarks and corresponding predicted landmarks. Then, the average of distance errors on each landmarks has been considered.

The results have been shown that using the convolutional network to predict the landmarks on biological images leads to satisfying results without need for segmentation step on the object of interest. The best set of estimated landmarks has been obtained after a step of fine-tuning using the whole set of images that we have for the project, i.e. about all beetle parts. The quality of prediction allows using automatic landmarking to replace the manual ones.

References

[1] Y. LeCun, L. Bottou, Y. Bengio, P. Haffner, Gradient-based learning applied to document recognition, Proceedings of the IEEE 86 (11) (1998) 2278–2324.

[2] A. Krizhevsky, I. Sutskever, G. E. Hinton, Imagenet classification with deep convolutional neural networks, in: Advances in neural information processing systems, 2012, pp. 1097–1105.

[3] C. Szegedy, et al., Going deeper with convolutions, Cvpr, 2015.

[4] C. Farabet, C. Couprie, L. Najman, Y. LeCun, Learning hierarchical features for scene labeling, IEEE transactions on pattern analysis and machine intelligence 35 (8) (2013) 1915–1929.

[5] H. Li, Z. Lin, X. Shen, J. Brandt, G. Hua, A convolutional neural network cascade for face detection, in: Proceedings of the IEEE Conference on Computer Vision and Pattern Recognition, 2015, pp. 5325–5334.

[6] S. Palaniswamy, N. A. Thacker, C. P. Klingenberg, Automatic identification of landmarks in digital images, IET Computer Vision 4 (4) (2010) 247–260.

[7] C. Cintas, et al., Automatic ear detection and feature extraction using geometric morphometrics and convolutional neural networks, IET Biometrics 6 (3) (2016) 211–223.

[8] D. G. Lowe, Distinctive image features from scale-invariant keypoints, International journal of computer vision 60 (2) (2004) 91–110.

[9] H. Bay, T. Tuytelaars, L. Van Gool, Surf: Speeded up robust features, in: European conference on computer vision, Springer, 2006, pp. 404–417.

[10] Z. Liu, S. Yan, P. Luo, X. Wang, X. Tang, Fashion landmark detection in the wild, in: European Conference on Computer Vision, Springer, 2016, pp. 229–245.

[11] Y. Sun, X. Wang, X. Tang, Deep convolutional network cascade for facial point detection, in: Proceedings of the IEEE conference on computer vision and pattern recognition, 2013, pp. 3476–3483.

[12] Z. Zhang, et al., Facial landmark detection by deep multi-task learning, in: European Conference on Computer Vision, Springer, 2014, pp. 94–108.

[13] J. Yosinski, J. Clune, Y. Bengio, H. Lipson, How transferable are features in deep neural networks?, in: Advances in neural information processing systems, 2014, pp. 3320–3328.

34

[14] Y. LeCun, Y. Bengio, G. Hinton, Deep learning, Nature 521 (7553) (2015) 436–444.

[15] T. Mikolov, et al., Strategies for training large scale neural network language models, in: Automatic Speech Recognition and Understanding (ASRU), 2011 IEEE Workshop on, IEEE, 2011, pp. 196–201.

[16] G. Hinton, et al., Deep neural networks for acoustic modeling in speech recognition: The shared views of four research groups, IEEE Signal Processing Magazine 29 (6) (2012) 82–97.

[17] S. Jean, K. Cho, R. Memisevic, Y. Bengio, On using very large target vocabulary for neural machine translation, arXiv preprint arXiv:1412.2007.

[18] I. Sutskever, O. Vinyals, Q. V. Le, Sequence to sequence learning with neural networks, in: Advances in neural information processing systems, 2014, pp. 3104–3112.

[19] R. Collobert, J. Weston, L. Bottou, M. Karlen, K. Kavukcuoglu, P. Kuksa, Natural language processing (almost) from scratch, Journal of Machine Learning Research 12 (Aug) (2011) 2493–2537.

[20] R. Collobert, J. Weston, A unified architecture for natural language processing: Deep neural networks with multitask learning, in: Proceedings of the 25th international conference on Machine learning, ACM, 2008, pp. 160–167.

[21] M. D. Zeiler, R. Fergus, Visualizing and understanding convolutional networks, in: European conference on computer vision, Springer, 2014, pp. 818–833.

[22] K. Simonyan, A. Zisserman, Very deep convolutional networks for large-scale image recognition, arXiv preprint arXiv:1409.1556.

[23] K. He, X. Zhang, S. Ren, J. Sun, Deep residual learning for image recognition, in: Proceedings of the IEEE conference on computer vision and pattern recognition, 2016, pp. 770–778.

[24] S. Huang, M. Gong, D. Tao, A coarse-fine network for keypoint localization, in: The IEEE International Conference on Computer Vision (ICCV), Vol. 2, 2017.

[25] C. Szegedy, W. Liu, Y. Jia, P. Sermanet, S. Reed, D. Anguelov, D. Erhan, V. Vanhoucke, A. Rabinovich, Going deeper with convolutions, corr abs/1409.4842, URL http://arxiv. org/abs/1409.4842.

[26] D. Ciregan, U. Meier, J. Schmidhuber, Multi-column deep neural networks for image classification, in: Computer Vision and Pattern Recognition (CVPR), 2012 IEEE Conference on, IEEE, 2012, pp. 3642–3649.

[27] N. Srivastava, G. E. Hinton, A. Krizhevsky, I. Sutskever, R. Salakhutdinov, Dropout: a simple way to prevent neural networks from overfitting., Journal of machine learning research 15 (1) (2014) 1929–1958.

[28] Y. LeCun, K. Kavukcuoglu, C. Farabet, Convolutional networks and applications in vision, in: Circuits and Systems (ISCAS), Proceedings of 2010 IEEE International Symposium on, IEEE, 2010, pp. 253–256.

[29] Y. A. LeCun, et al., Efficient backprop, in: Neural networks: Tricks of the trade, Springer, 2012, pp. 9–48.

[30] J. Han, C. Moraga, The influence of the sigmoid function parameters on the speed of backpropagation learning, in: International Workshop on Artificial Neural Networks, Springer, 1995, pp. 195–201.

[31] V. Nair, G. E. Hinton, Rectified linear units improve restricted boltzmann machines, in: Proceedings of the 27th international conference on machine learning (ICML-10), 2010, pp. 807–814.

[32] S. Dieleman, et al., Lasagne: First release. (Aug. 2015). `doi:10.5281/zenodo.27878`.
URL `http://dx.doi.org/10.5281/zenodo.27878`

[33] P. et al, Scikit-learn: Machine learning in python, Journal of machine learning research 12 (Oct) (2011) 2825–2830.

[34] L. Torrey, J. Shavlik, Transfer learning, Handbook of Research on Machine Learning Applications and Trends: Algorithms, Methods, and Techniques 1 (2009) 242.

[35] J. Deng, et al., ImageNet: A Large-Scale Hierarchical Image Database, in: CVPR09, 2009.

[36] J. Margeta, et al., Fine-tuned convolutional neural nets for cardiac mri acquisition plane recognition, Computer Methods in Biomechanics and Biomedical Engineering: Imaging & Visualization 5 (5) (2017) 339–349. `arXiv:https://doi.org/10.1080/21681163.2015.1061448`, `doi:10.1080/21681163.2015.1061448`.
URL `https://doi.org/10.1080/21681163.2015.1061448`

[37] V. L. Le, M. Beurton-Aimar, A. Krahenbuhl, N. Parisey, MAELab: a framework to automatize landmark estimation, in: WSCG 2017, Plzen, Czech Republic, 2017.
URL `https://hal.archives-ouvertes.fr/hal-01571440`